MEASUREMENT OF CHANGES IN ATMOSPHERIC Ar/N_2 RATIO USING A RAPID-SWITCHING, SINGLE-CAPILLARY MASS SPECTROMETER SYSTEM.

Ralph F. Keeling[1*]
Tegan Blaine[1]
Bill Paplawsky[1]
Laura Katz[1]
Chris Atwood[1]
Tim Brockwell[2]

[1]Scripps Institution of Oceanography, La Jolla, CA 92093-0244 USA
[2] GV Instruments, Crewe Road, Wythenshawe, Manchester M23 9BE UK

[*]Corresponding author: rkeeling@ucsd.edu

DRAFT: 3 JAN 2004

ABSTRACT

The atmospheric Ar/N_2 ratio is expected to undergo very slight variations due to exchanges of Ar and N_2 across the air-sea interface driven by ocean solubility changes. Observations of these variations may provide useful constraints on large-scale fluxes of heat across the air-sea interface. A mass spectrometer system is described that incorporates a magnet with a wide exit face, allowing a large mass spread, and incorporates an inlet with rapid (5s) switching of sources gases through a single capillary, thus achieving high precision in the comparison of sample and reference gases. The system allows simultaneous measurement of Ar/N_2, O_2/N_2 and CO_2/N_2 ratios. The system achieves a short-term precision in Ar/N_2 of 10 per meg for a 10-second integration, which can be averaged to achieve an internal precision of a few per meg in the comparison of reference gases. Results for Ar/N_2 are reported from flasks samples collected from 9 stations in a north-to-south global network over about a 1 year period. The imprecision on an individual flask, as estimated from replicate agreement, is ±11 per meg. This imprecision is dominated by real variability between samples at the time of analysis. Seasonal cycles are marginally resolved at the extra-tropical stations with amplitudes of 5 to 15 per meg. Annual-mean values are constant between stations to within ± 5 per meg. The results are compared to a numerical simulation of the cycles and gradients in Ar/N_2 based on the TM2 tracer transport model in combination with air-sea Ar and N_2 fluxes derived from climatological air-sea heat fluxes. The possibility is suggested that Ar/N_2 ratios may be enriched detectably near the ground by gravimetric or thermal diffusion under conditions of strong surface inversions.

1. INTRODUCTION

The oceans play a major role in global climate through their ability to absorb and release heat. Every year, the oceans transport around 60 ZJ (Zetajoule = 10^{21}J) from lower to higher latitudes in each hemisphere, thus moderating the climate differences between equator to poles; and each spring and summer the oceans at middle and high latitudes absorb around 150 ZJ and return an equivalent amount of heat to the atmosphere in the fall and winter, thus reducing the temperature contrast between summer and winter (Peixoto and Oort, 1992). The oceans are also believed to be slowing the atmospheric response to increasing greenhouse gases by absorbing around 10 ZJ globally each year (Levitus et al., 2000; Levitus et al., 2001). The magnitude of these heat flows, however, is still subject to considerable uncertainty, and the variations in these flows from year to year are not easily measured, which reduces our ability to make reliable climate forecasts on various time scales.

The need for improved determinations of air-sea heat flux has fueled the development of new measurement methods, such as technologies for expanding the coverage of ocean temperature measurements (Gille, 2002), and methods based on acoustic tomography (Baggeroer et al., 1998; Munk and Wunsch, 1979) and satellite altimetry (Cabanes et al., 2001). This need has also stimulated interest in developing a method based on measuring changes in atmospheric composition, specifically the relative abundances of N_2 and the inert gases Xe, Kr, Ar, Ne, and He in the atmosphere. These gases are sufficiently unreactive that the total burden of each gas in the combined ocean/atmosphere system is constant to a very high level. The partitioning of these gases between the ocean and the atmosphere is, however, sensitive to ocean temperature, via the temperature-dependence of the solubility (Craig and Wiens, 1996). Warmer water tends

to hold less gas than colder water, so heating of the oceans results in a net release of gas to the atmosphere, while cooling causes a net uptake. This temperature effect is more pronounced for the heavier of these gases, which have Bunsen solubilities that are larger and more strongly dependent on temperature. The ratio of the heavy to light gases in the atmosphere (Xe/Ar, Kr/N_2, Ar/N_2, etc.) should therefore increase in response to ocean warming and decrease in response to ocean cooling. The effect of water temperature on the dissolved gas abundances has been exploited in paleoclimate studies (e.g. Stute et al., 1995) but the reciprocal effect on atmospheric abundances remains largely unexplored.

Hydrographic surveys (Craig et al., 1967; Hamme and Emerson, 2002) and time series studies (Schudlich and Emerson, 1996; Spitzer and Jenkins, 1989) confirm that most of variability in dissolved N_2 and the heavier inert gases is explained by the temperature dependence of the solubility. Solubility control is expected based on the relevant time scales: dissolved gases within the ocean mixed layer equilibrate with the atmosphere on a typical time scale of days to a few weeks, which is shorter than the typical time scale of months for the mixed layer to undergo substantial temperature changes. For a gas to remain near solubility equilibrium in spite of warming and cooling, it is a requirement that the air-sea fluxes of these gases be governed, to a first approximation, by (Keeling et al., 1993):

$$F_i = P_i \, (-dS_i/dT) \, Q/C_p \qquad (1)$$

where F_i (mol m^{-2} yr^{-1}) is the net flux (positive into the air) of gas species *i*, P_i (atm) is the partial pressure of species *i* in air, dS_i/dT (mol m^{-3} atm^{-1} $^{\circ}C^{-1}$) is the temperature derivative of the Bunsen

solubility, Q (J m^{-2} yr^{-1}) is the net heat flux into the water (sum of latent heat, sensible heat, longwave, and shortwave components), and C_p is the heat capacity of seawater (J m^{-3} $^{\circ}C^{-1}$).

In Table 1, we have estimated via Eq. (1) the change in the total atmospheric burden of N_2 and the inert gases for a heat input to the ocean of 100 ZJ. The change is larger for heat input into colder water, because the solubility derivatives ($-dS_i/dT$) are larger at low temperatures. From Table 1, an input of 100 ZJ into a 10°C ocean water mass which maintains solubility equilibrium would release enough Kr, Ar, and N_2 to increase the total atmospheric burden of these gases by 0.00104%, 0.00043%, and 0.00017%, respectively. If the excess were mixed uniformly throughout the entire atmosphere, this would increase in the Kr/N_2 ratio by 0.00104%-0.00017% = 0.00087% and the Ar/N_2 ratio by 0.00043%-0.00017% = 0.00026%. It is customary to express such small changes in "per meg" units, for example

$$\delta(Ar/N_2)\ (\text{per meg}) = \left((Ar/N_2)_{sample}/(Ar/N_2)_{reference} - 1 \right) \times 10^6 \qquad (2)$$

so that a change of 0.00026% is expressed as 2.6 per meg.

Changes in relative atmospheric inert gas abundances are expected both globally and locally. At a given location, the atmospheric inert gas abundances will depend on the magnitude of air-sea heat exchanges, kinetic rates of air-sea exchange, and rates of atmospheric mixing. The largest expected changes are quasi-regular seasonal cycles at middle and high latitude tied to seasonal cycle of ocean heat storage. Based on model simulations using different heat-flux and heat storage climatologies (Gibson et al., 1997; Samuels and Cox, 1987) and several atmospheric transport models (Heimann, 1995; Tans et al., 1989), and assuming the validity of Eq. (1), we

estimate that the atmospheric Ar/N_2 ratio should exhibit seasonal variations at sea-level in middle and high latitudes of order 10 to 20 per meg. These cycles are likely superimposed on gradients in annual-mean concentration between low and high latitudes at sea level and between the northern and southern hemispheres of the order of a few per meg associated with ocean meridional heat transport. The cycles are also expected to be superimposed on a long-term increase in the Ar/N_2 ratio of around 3 per meg per decade caused by global warming.

This paper reports progress in a program at the Scripps Institution of Oceanography to measure changes in the atmospheric Ar/N_2 ratio. The Ar/N_2 ratio has the advantage that both gases are relatively abundant in air, allowing the use of small (~several liter) air samples. Although ratios involving the heavier gases (e.g. Kr/N_2 and Xe/N_2) would be more sensitive to heat exchanges, their measurement (e.g. via isotope dilution) would require much larger samples and additional processing to concentrate the inert gas prior to analysis. We have focused on Ar/N_2 primarily because the measurement is feasible using flasks already being collected for interferometric O_2/N_2 measurements at Scripps (Keeling et al., 1998).

Our study parallels that of Battle et al. (2003), which was the first study to document significant variations in the Ar/N_2 of the atmosphere. The Battle et al. study presented data over a 3-year period from six stations distributed globally and demonstrated that the Ar/N_2 ratio indeed varies seasonally, with roughly the magnitude expected based on seasonal air-sea heat exchanges. The Battle et al. study further illustrates the usefulness of such data for constraining coupled models of the ocean/atmosphere system. The study also shows the need for improving measurement precision and eliminating sampling biases, which limit the usefulness of the existing data.

Our approach, like that of Battle et al (2003), involves using a multi-collector mass spectrometer for whole-air analysis, as pioneered by Bender et al (1994) for O_2/N_2 measurements. We apply this approach using a wide-sector mass spectrometer that allows for simultaneous measurement of O_2/N_2, CO_2/N_2 and Ar/N_2 ratios. The mass spectrometer incorporates an inlet system in which sample and reference gases are switched upstream of a single inlet capillary. Leuenberger et al. (2000) recently describe a system that bears some similarity to that described here. Our approach differs from that of Leuenberger et al. principally in allowing for higher beam strengths and more rapid sample/reference switching, thus further increasing precision.

Here we describe our method in some detail and describe tests we have performed to assess the system performance. We also describe results for Ar/N_2 from flasks collected from stations in a global north-south network over roughly a 1-year period.

2. METHODS

2.1 Mass Spectrometer System

We use a Micromass Isoprime mass spectrometer, which is configured with 8 collectors (Table 2) that can be integrated simultaneously, thus allowing 3 distinct elemental ratios (Ar/N_2, O_2/N_2, CO_2/N_2) and 4 distinct isotopic ratios (^{15}N-$^{14}N/^{14}N$-^{14}N, ^{15}N-$^{15}N/^{14}N$-^{14}N, ^{18}O-$^{16}O/^{16}O$-^{16}O, $^{36}Ar/^{40}Ar$) to be measured simultaneously in an air sample. Our focus here is exclusively on the elemental ratios, with particular emphasis on Ar/N_2. The IsoPrime employs an asymmetric analyzer geometry with an effective radius of 108mm. The wide exit face of the electromagnet enables a mass spread of 62% to be utilized on the focal plane of the instrument, allowing the

simultaneous measurement of masses 28 to 44, as shown in Figure 1. The analyzer housing employs an open design in which the source, flight-tube, and detector elements are incorporated into a single rectangular vacuum vessel, thus providing mechanical rigidity as well as an unrestricted flight tube permitting the wide mass spread. The open design of the flight tube also allows for efficient evacuation by a single turbomolecular pump, which reduces the instrumental non-linearity. An electron impact source is used, fitted with a thoriated-iridium filament for sensitivity. The collector array is composed of deep Faraday cups. Each collector has a slit width designed so that, in normal use, the beam from each monitored mass falls entirely within the collector.

The native control software for the IsoPrime is MassLynx, which controls all aspects of instrument tuning, operation and data acquisition. The highly specific nature of the data processing requirements of this application has driven the development of a suite of software written in the LabView programming language. This Labview software controls MassLynx via a number of ActiveX and COM interfaces. The interfacing involves the Labview program sending commands to MassLynx at 10 minute intervals, and retrieving the collector signals nearly real time with 100ms resolution. The LabView software further processes the collector signals to compute “initial” delta values (described below) at 10 second intervals, which in turn are displayed graphically and stored in output files.

The measurement of isotope or elemental ratios via mass spectrometry typically requires switching between sample and reference gases in order to cancel instrument drift. With traditional inlet systems, however, the rate at which gases can be switched - and thus the degree to which instrument drift can be canceled - is limited by the need to allow the ion source to

recover from pressure transients caused by switching. This typically limits the switching rate to 15 seconds or longer. Measurement precision may also be degraded by imbalances between sample and reference gas pressure, which can lead to biases due to non-linear source effects (Bender et al., 1994; Leuenberger et al., 2000).

Here we overcome these limitations by employing the custom inlet system shown in Figure 2. This system employs the standard Micromass changeover valve, operated here with inlet flows of 10 to 20 SCCM and outlet pressures of ~0.4 atm. The output of one side of the changeover valve is directed to a "T", which allows a small fraction of the flow (~0.01 STP mL min^{-1}) to be delivered via a crimped stainless-steel capillary into the mass spectrometer source. The remainder of the gas delivered through this exhaust port is wasted to a vacuum pump. The output of the other side of the changeover valve is similarly wasted to the same vacuum pump. The pressures and flows upstream of the changeover valve are equalized via active electronic pressure control and by adjusting flow restrictions (manual flow control valve and crimp), thus effectively reducing the pressure fluctuations downstream of the changeover valve caused by switching. Small residual fluctuations at the capillary inlet are further suppressed via an additional stage of active pressure control downstream of the changeover valve. A Licor non-dispersive infra-red (NDIR) CO_2 analyzer, which also takes advantage of the pressure-control scheme, is incorporated upstream of the changeover valve. The NDIR provides a measure of CO_2 concentration that is largely redundant to that based on the M/Z = 44 and M/Z = 28 ion currents. One input port of the change-over valve is connected to a fixed instrument reference gas, which also serves as reference gas for the NDIR analyzer. The other input port allows the introduction of samples and reference gases as described further below.

An example of the mass spectrometer output is shown in Figure 3. Here the changeover valve is switching at 5-second intervals, alternately allowing the instrument reference gas versus sample gas into the mass spectrometer. These two gases have well-resolved differences in CO_2 concentration (44/28) and in O_2/N_2 ratio (32/28) but not in Ar/N_2 ratio (40/28). The time scale for replacing one gas with the next is seen most clearly from the 44/28 ratio signal: there is a ~1 second delay between the switch and the initial arrival of new gas, and an additional ~1 second is required for the exchange of gases to progress to 90% completion. There is no indication of any pressure transients in the replacement of one gas with the next.

With the 5-second switching scheme, the concentration difference between the sample and instrument reference gas can be determined with 10-second resolution. We denote this difference, which we compute based on the raw ratio signals (see Figure 3) with the symbol δ_i (*i* for "instrument"). Under typical conditions, δ_i is determined every 10 seconds to a precision of 10 per meg (1σ) in the 40/28 ratio, 4 per meg in the 32/28 ratio, and 60 per meg in the 44/28 ratio. Based on sensitivity tests with known CO_2 additions, described below, the 44/28 precision corresponds to 0.03 μmol/mol in the CO_2 mole fraction.

2.2 Instrument Noise Spectrum

While the 5-second switching sequence effectively cancels detector drift on time scales longer than ~10s, considerable noise remains on shorter time scales. Could faster switching rates reduce this noise? To assess this question we introduce a steady stream of one gas into the mass spectrometer without switching at all. We then process the collector signals as if switching had occurred, to compute differences δ_i between consecutive segments. We carry out this processing

for variable (hypothetical) switching period as well as for variable "dead time", i.e. the time window over which the signals are discarded to allow for stabilization after the switch (also known as "idle time"). From these data, we compute the standard error in δ_i over a 20-minute interval. This we compute according to $\sigma_i/(N)^{1/2}$, where N is the number of (hypothetical) reference-sample-reference jogs of one polarity that fit into 20 minutes and where $\sigma_i = ((\Sigma(\delta_i)^2)/N)^{1/2}$. The summation is carried over the N jogs, and δ_i for each jog is computed by averaging the 0.1s mass spectrometer output over the sample and reference segments and interpolating between reference segments, as per Figure 3. (Note that because the ensemble mean is known to be zero *a priori*, the observed mean value of δ_i is not subtracted in the expression for σ_i, and N is used in the denominator, rather than N-1.) This analysis, carried out for variable switching periods, is roughly equivalent to computing the noise power spectrum.

The results, shown in Figure 4, show several interesting features. Focusing on the results with a short dead time of 0.3 seconds, we see that the standard error improves as the switching rate is increased, consistent with the improved cancellation of slow instrument drift and consistent with the mass spectrometer having a red noise spectrum at low frequencies. At high switching rates, however, the standard error becomes independent of switching rate, consistent with a white spectrum at high frequencies. In this limit, the performance is limited by the shot noise or Poisson counting statistics from the ion currents. As the figure shows, however, achieving this limit requires having a short dead time. With longer dead times, the precision degrades if the switching is too rapid, as a large fraction of the data is then being discarded. For a dead time of 10 seconds, the optimum switching period is around 20 seconds, corresponding to retaining half the data. For a dead time of 1 second, the optimum switching

period is around 5 seconds, with a very broad optimum that is close to the shot-noise limit.

Comparing results for the two dates in Figure 4, we see that the performance at slower switching rates can vary from day to day, presumably as a result of changes in instrument tuning, filament conditions, or external environmental parameters. At higher switching rates, however, the performance is anchored near the statistical limit. Comparing results for the different ion ratios, we find that the optimum switching rate (for a given dead time) is slightly faster for 32/28 than for 40/28, consistent with the former having higher beam strength, smaller shot noise, and hence a larger relative contribution from red or "flicker" noise.

Our standard operating conditions, with actual gases being switched, employs a switching rate of 5 seconds and allows for ~2 seconds of dead time, after a 1 second delay. According to Figure 4, we would expect the performance under these conditions to be within a factor of two of the statistical limit. Our results comparing two gases confirm this expectation, showing that little additional noise is introduced by the switching of the valve itself and implying that only a rather modest improvement in performance would be achieved by faster switching, by itself. Further noise reduction could potentially be achieved, however, by a combination of faster switching and increasing the beam strengths.

2.3 Gas Handling

For a number of years, the O_2 laboratory at Scripps has employed a system for analyzing flask samples for O_2/N_2 ratios and CO_2 concentrations using a custom interferometer and a Siemens Ultramat 3 NDIR CO_2 analyzer. This system, described in detail in Keeling et al. (1998), is calibrated using reference gases derived from high pressure cylinders, which are

introduced via a manifold upstream of both analyzers.

We have now interfaced the mass spectrometer in such a way that it is fed by the same calibration gases. This was done using a pickoff "T" upstream of the NDIR and interferometric analyzer, which allows calibration gases to be compared in parallel on both systems. The T operates at the regulator delivery pressure of around 10 PSIG. To minimize the potential for thermal fractionation at the T, we employ a concentric design suggested by M. Bender, in which the pick-off flow is derived from a smaller bore tubing that is aligned axially within the larger bore of the main (bypass) flow. Temperature gradients are further reduced by embedding the T in a machined brass block that, in turn, is embedded in insulation. It is possible that the T may still fractionate due to orifice effects, but we expect such fractionation would be constant with time, and thus have the effect of inducing a constant offset between the Ar/N_2 ratios reported on tanks versus flasks. We have not tried to correct our data for any such effect at this time.

Downstream of the pick-off T, we have introduced a new manifold system for mass-spectrometric analysis of flask samples, as shown in Figure 5. This system incorporates (1) a multi-port rotary valve (Valco Instruments, Inc.) for introducing flasks, (2) a vacuum system for purging and evacuating flask lines, (3) a "direct inlet gas" for maintaining stable operating conditions in the mass spectrometer during preparations for flask analysis, and (4) active pressure control for matching the reference gas delivery pressure to that in individual flasks, thereby minimizing pressure changes when flask air is introduced. Although the manifold has 16 positions, only four positions are used for our normal 5-l flasks due to space constraints. The manifold system incorporates a thermal enclosure surrounding the flasks and the proximate bypass valves. The manifold includes magnetic stirrers for mixing the air in the 5l flasks during

analysis. The motor units for driving the magnets are located outside the thermal enclosure, with only a rotating shaft penetrating the enclosure.

The setup allows flasks to be analyzed either in a "purge" mode, in which both the inlet and outlet ports of the flasks are opened and the flask air is diluted with tank air during analysis, or alternately in a "sniff" mode, in which only the outlet port of the flask is connected and the flask pressure decreases during analysis. The latter mode was used for all results presented here. In this mode, two lines are connected to each flask at a single specially-designed ball and socket joint, to allow purging of all lines up to this joint prior to analysis.

The preparation sequence starts by inserting stir-bars into the flasks and connecting the flasks at this ball joint. We then purge the connections with dry air, first at a flow rate of around 200 ml min^{-1} and then at the nominal analysis flow of 15 ml/min, while monitoring the mass spectrometer and CO_2 analyzer output to ensure complete removal of room air or diagnose leaks. At completion of the purge, each flask position is then evacuated for 1 minute and the sample loop is isolated at the flask bypass valve. The manual purge valve is then closed and the flask stopcock opened, resulting in backfill of the loop with sample. After a short equilibration time, the pressure of the flask is recorded and the flask select valve is advanced to the next flask position, where the procedure is repeated. Unused ports are capped off and treated as if they contained flasks to reduce cross-port contamination during switching. Once this preparation sequence has been completed for all flasks, the thermal insulated enclosure, which houses all flasks, is then sealed, the stir-bars are activated, and 30 minutes is allowed to elapse before proceeding. During this time, working gas flow is maintained into the mass spectrometer via the flask bypass valve.

At the start of each analysis, the flask select valve moves to a mounted position (still isolated via the flask bypass valve) and the working gas pressure is adjusted with an active pressure controller to agree with the flask pressure determined earlier. The working gas is analyzed at this pressure to establish a leading baseline, whereupon the flask bypass valve is switched to introduce flask air, effectively stopping the working gas flow through the bypass valve. (Working gas flow is maintained, however, into the interferometer, via the other branch of the T.) The analysis continues for 10 minutes at which point the flask pressure will have dropped nominally by ~31 mb. The bypass valve is switched to re-introduce working gas, thus establishing a trailing baseline.

Our air samples are collected in 5-l glass flasks equipped with Viton O-rings which are flushed in the field with a freeze-dried air-stream. At stations near sea level, the pressure in the flasks is maintained just above ambient barometric pressure via an open exhaust line. At the high elevation stations (Mauna Loa, South Pole) the pressure is maintained near ~1 atmosphere via a back-pressure regulator located near the outlet of the exhaust line, separated from the flasks by several meters of tubing. The air is dried to a dew point between -45EC and -80EC, depending on the station. Flasks are typically collected in triplicate, either serially in time, or simultaneously as a serially-flushed string of three, depending on the sampling station. At all stations other than Kumukahi, flasks are sampled indoors, in order to minimize thermal gradients, with the intake line extending to a nearby high point or tower outside. At Kumukahi, the flasks are collected outdoors under a portable shade, to reduce solar heating. Starting in the summer of 2001, we began analyzing two of three replicates on the mass spectrometer system in sniff mode prior to analysis on the interferometer system. The third flask was analyzed only on

the interferometer system. This approach provides a measurement of Ar/N_2 ratios and redundant measurements of CO_2 and O_2/N_2 on two out of three flask replicates.

Flasks are typically analyzed against the gas delivered from a working tank (WT), and the working tank is analyzed on a daily basis against a series of secondary reference gases, or "secondaries" (A and B). A typical sequence is shown in Figure 6.

Reference gases are pumped at Scripps and dried to the level of ~2 μmol mol^{-1} H_2O or better using a molecular sieves. During usage, all reference and working tanks are laid on their side and placed in an insulated enclosure. Within the enclosure, the end-to-end (horizontal) temperature gradients of the tanks is typically of order ~0.02 EC. The tank regulators are located outside the enclosure and connected to the cylinder head valves via 1/16" O.D. nickel lines. See Keeling et al. (1998) for further details.

2.4 Calibration

We compute changes in Ar/N_2 from the mass spectrometer raw signals in several steps, with the net effect being a transformation of the form

$$\delta(Ar/N_2) = a\ \delta_i(40/28) + b\ \delta_i(32/28) + c\ \delta_i(44/28) + d \qquad (3)$$

where *a* accounts for the combined influence of the intrinsic sensitivity of the mass spectrometer (i.e. non-linearity) and incomplete sample/reference replacement during switching ("cross-over contamination"), *b* and *c* account for interferences due to isobaric effects or ion-molecule chemistry, and *d* accounts for variations in the composition of the instrument reference gas,

working gas, and the additional reference gases.

Coefficients *a*, *b*, and *c* were established in August, 2001 by recording the mass spectrometer response as a function of known changes in gas composition. The gas composition was altered by bleeding variable amounts of a prepared gas mixture into a reference gas stream and analyzing the resulting mixture. The prepared gas mixture consisted either of (1) pure CO_2, (2) a gravimetric mixture of O_2 and CO_2, or (3) a gravimetric mixture of Ar and CO_2. The relative proportions of the reference gas and the prepared gas were determined by measuring changes in CO_2 mole fraction on a well-calibrated CO_2 system (Keeling et al., 1998). The addition of pure CO_2 allowed the coefficient *c* to be measured. Coefficients *a* and *b* were computed based on results for the other two gas mixtures, after subtracting the influence of CO_2 on the beam ratios. These tests showed that *b*=0 to within uncertainties, that *c* is consistent with a weak isobaric interference on mass 28 due to CO^+, and that *a* is consistent with a cross-over contamination effect of several percent and an intrinsic non-linearity of less than 2%. Variations in *a* and *c* relative to August, 2001 are determined based on a span normalization factor, derived based on the apparent changes of a tank prepared with relatively large differences in Ar/N_2, O_2/N_2 and CO_2/N_2.

Coefficient *d* is established based on a hierarchical scheme of reference gas comparisons. Briefly, the $\delta_i(40/28)$ values for flasks samples are subtracted from the $\delta_i(40/28)$ values of the working gas (WT) and the resulting difference is added to an assigned value for the working gas. The working-gas assignment is made on a daily basis, based on comparison with the "secondaries" (see Figure 6, segments A and B). The results are then adjusted for sensitivity and interference effects (coefficients a, b, and c in Equation 3) and a time-varying additive

adjustment is made (via d) to maintain constancy in the δ values of a suite of primary reference gases, or "primaries". The primaries are analyzed using essentially the same procedures and algorithms as flask samples. The procedure assumes that the primaries are stable over the long term. Unlike the common practice for reporting isotopic ratios, the zero value of the $\delta(Ar/N_2)$ scale does not necessarily correspond to the concentration of an actual reference material. The redundancy inherent in this approach is advantageous in producing a scale with long-term stability. We have used the same approach for maintaining an $\delta(O_2/N_2)$ scale in our lab; see Keeling et al. (1998) for additional details.

Working gases typically last several months and are replaced when their pressure drops ~800 kPa, while the secondaries typically last a year or more and are replaced when their pressures drop to about 3300 kPa. Procedures for replacing these gases in a self-consistent manner are described in Keeling et al. (1998). Primaries are used sparingly in order to last decades without significant depletion.

3. PERFORMANCE TESTS

3.1 Thermal fractionation

In the course of conducting tests of the performance of our system, we have found that a ubiquitous challenge is the need to minimize thermal fractionation of samples and reference gases. To aid in subsequent discussions, we digress briefly here to present estimates of the relevant thermal fractionation factors for O_2/N_2 and Ar/N_2 in air. Table 3 summarizes literature estimates of thermal diffusion factor α, thermal diffusion sensitivity Ω, and diffusivity D for Ar

and O_2 in air. Ω is computed according to $(\alpha/T)\times10^6$ (per meg/EC), where T is the temperature in degrees Kelvin (Severinghaus et al., 2001). Table 3 also summarizes estimates of the ratio of αD for Ar/N_2 versus αD for O_2/N_2 both from literature and as recently measured in our lab.

The thermal diffusion factor α and sensitivity Ω are measures of the steady-state concentration gradient that is induced by a temperature gradient in the absence of bulk flow. In contrast, the product αD, is a measure of the fractionating flux under transport-limited conditions, as is commonly the case in the presence of bulk flow. We expect that under most conditions relevant to our laboratory and field operations, any thermal fractionation will scale more nearly in proportion to αD rather than to α.

We have measured the ratio αD for Ar/N_2 versus αD for O_2/N_2 (i.e. $(\alpha D)_{Ar/N2}/(\alpha D)_{O2/N2}$) by divided a flowing gas stream at a "T" junction while slightly heating one branch of the T and measuring differences in Ar/N_2 and O_2/N_2 between the two branches of the T directly on the mass spectrometer. We found that the differences in Ar/N_2 between the branches of the T were highly correlated to differences in O_2/N_2, and we interpret the slope of the correlation plot as measuring $(\alpha D)_{Ar/N2}/(\alpha D)_{O2/N2}$. The experiment was carried at pressures of 1 atm and 120 atm, the latter being characteristic of pressures in high-pressure gas cylinders. The results, presented in Table 3, clearly establish that the ratio $(\alpha D)_{Ar/N2}/(\alpha D)_{O2/N2}$ is pressure dependent, with lower values at higher pressures.

3.2 Tank Stability

A useful measure of the performance of our analysis system is provided by the daily value of the working gas, which is determined each day that flasks or reference gases are

analyzed. A composite history of eight working gases is shown in Figure 7a. The working-gas Ar/N_2 ratios fluctuate on a day-to-day basis by ~±2 per meg, which is about twice the value expected based on the imprecision in δ_i, indicating that some day-to-day variability results from imperfect gas handling. Superimposed on these fluctuations is a downward trend in Ar/N_2 that is detectible in most tanks. The change from first to last analysis on a given working gas ranges from !2 to !27 per meg, with an average of -13 per meg. The drift seems to accelerate near the point the tank is used up and is possibly also faster for some tanks at the very onset of usage. Discarding the first and last analyses, the drift ranges from 0 to !12 per meg, with an average of !7 per meg. The working-gas drift must be a consequence of gas usage, because it is assessed relative to the secondaries, which differ from the working tank only in being depleted less rapidly.

As shown in Figure 7b, the WT variations in Ar/N_2 are well correlated with variations in O_2/N_2 at a ratio of around 2.5:1. This small effect in WT O_2/N_2 ratios was not noticed previously (Keeling et al., 1998), and came to our attention only in light of the more obvious changes in Ar/N_2. The effect may have become more pronounced after our laboratory moved to a new building in 1999. We believe the effect is likely caused by thermal fractionation in the tanks, as the ratio of 2.5 is close to the ratio of 2.17 which we measured for $(\alpha D)_{Ar/N2}/(\alpha D)_{O2/N2}$ at a typical tank pressure of 120 atm.

The same depletion effect may influence our secondaries, although at a much slower rate due to their more limited usage. A typical shift of around !5 per meg in Ar/N_2 and !2 per meg in O_2/N_2 in the secondaries would be expected over their lifetime, considering the tanks are used only over a limited intermediate pressure range. We have not yet been able to verify this

predicted drift, due to the short time span of the Ar/N_2 measurements. In principle, such drift should be detectible via the comparisons with the primary reference gases, which are depleted even less rapidly.

3.3 Pressure-induced thermal fractionation

In the course of the initial testing of the flask manifold system, shown previously in Figure 5, some difficulty was encountered in generating stable Ar/N_2 and O_2/N_2 ratios from air delivered from flasks in sniff mode. The Ar/N_2 ratios would drift downwards by as much as 20 per meg within the 10-minutes analysis period. We have traced this effect to thermal diffusion within the flasks in the response to pressure-induced temperature changes. As the flask pressure drops during analysis, the air in the flask cools by adiabatic expansion, with the maximum cooling occurring near the center of the flask and the minimum occurring near the walls, due to the thermal buffering of the glass. The air exiting the flask is thus exposed to a thermal gradient which will deplete the Ar/N_2 ratio of the air exiting the flask relative to the average composition in the flask. Scale analysis suggest it should be possible to fractionate Ar/N_2 at the center of the flask by the order of 100 per meg relative to the walls, given the pressure drop (~3%), the thermal diffusion sensitivity of Ar/N_2 (~250 per meg/EC), the diffusivity of Ar in air at 20EC (~0.19 $cm^2 s^{-1}$), the flask radius (~15cm), and the time scale for our flask analyses (~10 min).

To better quantify this pressure-induced fractionation effect, we conducted tests in order to isolate the effect of dropping pressure on the composition of the air delivered from a flask. A flask was mounted on the manifold, the insulated enclosure was sealed, and the flask was purged with working gas until a stable baseline was achieved on the mass spectrometer. The inlet

stopcock of the flask was then closed (using a manual shaft that penetrated the insulation), while the outlet stopcock was left open, and the response of the mass spectrometer signal was noted as the flask pressure dropped. The test was done at our typical analysis flow rate of 15 ml min^{-1} with an initial flask pressure of 1 atm. This test was repeated four times, and a representative result is shown in Figure 8. Within a few minutes after closing the stopcock, the Ar/N_2 and O_2/N_2 ratios decreased, achieving lower quasi-stable baselines within about 5 minutes. The baseline shifts were highly reproducible. The baseline shifts in Ar/N_2 ratio averaged by -17±3 per meg, while the baseline shifts in O_2/N_2 averaged -4.5±0.4 per meg. The ratio (17±3)/(4.5±0.4) = 3.8±0.18 is consistent with the ratio of 3.77 which we measure for $(\alpha D)_{Ar/N2}/(\alpha D)_{O2/N2}$ at 1 atm pressure, thus pointing to thermal diffusion as the ultimate cause. We were able to reduce the effect by ~20% by stirring the air continuously in the flask with a magnetically driven stir-bar (as is done for our normal flask analyses). The stirring was insufficient to eliminate the effect, presumably because it induced regular circular motion without greatly enhancing the mixing between the center of the flask and the walls.

In a second test, we were able to demonstrate that the baseline shift is due to the pressure drop in the flask, rather than in the gas lines downstream of the flask. In this test, the flow was directed through the "flask select" valve and through the flask bypass valve, but the flask itself was closed. The pressure set point on the electronic pressure controller was then reduced at a steady rate mimicking the pressure drop for the flask run. This test produced no detectible baseline shift.

The pressure-induced thermal fractionation effect is evident in analysis of actual flask samples. In Figure 9, we have combined 520 separate flask analysis peaks by bin-averaging the

time-varying concentrations during analysis to produce a single high precision peak. The peak is characterized by a plateau in which the Ar/N_2 and O_2/N_2 ratios are quite stable, on average. This plateau, however, is preceded by a "hump" (before segment B) during which the O_2/N_2 and Ar/N_2 ratios are both elevated. By comparing peaks from flasks with different concentrations (not shown), we have verified that the hump is anchored relative to the flask plateau, and hence represents altered flask air rather than an altered residue of the working gas (or a mixture of the two). A synchronous hump of the same sign is seen in O_2/N_2 with a magnitude around 3.5 times smaller. A similar hump in Ar/N_2 is seen on the second working gas segment (before segment C), although this feature is less well correlated to changes in O_2/N_2. This second hump is almost certainly influenced by the stopping and restarting of the WT flow in the lines upstream of the flask, and thus has a different origin than the hump preceding segment B.

All the evidence points to the hump preceding segment B as resulting from the same phenomena as was isolated in our tests above. In other words, segment B represents flask air that has been thermally fractionated due to pressure-induced cooling, while the hump preceding segment B represents flask air that has been less fractionated. To compute flask concentrations, we rely only on the data within the stable segments (A,B,C) in Figure 9. We therefore expect that our flask results are likely biased low by ~14 per meg in Ar/N_2 (i.e. 80% of 17 per meg) relative to the initial concentration in the flasks. The flasks result presented below have not been corrected for this bias.

3.4 Flask Replicate Agreement

Another useful measure of performance is the level of agreement between replicate flasks

collected at the same place and time. Following Keeling et al. (1998), we compute differences between each flask and the replicate mean, and scale these residuals by a factor of $(N/(N-1))^{1/2}$, where N is the number of replicates. This scaling is used so that the standard deviation of the residuals is equal to that of the hypothetical parent distribution with an infinite number of replicates, and thus represents the imprecision that should be assigned to an individual flask measurement. A normal probability plot of scaled residuals for Ar/N_2 is shown in Figure 10a, which indicates that the residuals follow a normal distribution to a very good approximation. This plot is based on 520 flasks collected at our 9 sampling stations. The implied σ on an individual flask is ±11 per meg in Ar/N_2. In subsequent discussions, we refer to this σ based on residuals from replicate mean as the "uncorrelated error" σ_{uncor} to distinguish it from error which is shared by all members of a set of replicates. This latter we refer to as "correlated error" σ_{corr}. The residuals in Ar/N_2 among flask replicates are correlated with corresponding residuals in O_2/N_2 as shown in Figure 10b. Roughly 31% of the variability in Ar/N_2 is explained by variability in O_2/N_2 and vice versa. Most of the data cluster around a line with a slope of around 4:1 (Ar/N_2: O_2/N_2), which is consistent with the ratio expected from thermal fractionation at 1 atm pressure.

3.5 Flask Storage Tests

Finally, we conducted a limited test of the long-term stability of Ar/N_2 ratios in our flasks. The test involved purging the contents of several flasks plumbed in series at a flow of 1 l STP min^{-1} with air derived from a particular high pressure cylinder. The output of the final flask was vented to the room through a long section of tubing, to establish a pressure near 1

atmosphere in the flasks while avoiding the introduction of room air. The flasks stopcocks were then closed and the flasks were stored at ambient pressure in our normal shipping boxes. Two of these flasks were analyzed 98 days after the initial purge date, and three were analyzed 363 days after the purge date. The purge tank was also analyzed before and repeatedly after the date of fill, which established its concentration at the time of fill to around ±5 per meg. The observed Ar/N_2 ratios in the five flasks were all within a range of ±15 per meg of the tank concentration. There was no clear evidence of systematic drift in flask concentrations over time. By itself, this test probably sets an upper bound to any drift in our flasks of ~15 per meg in Ar/N_2 per year. Note that the flasks used for these storage tests, like the flasks collected for our program at field stations, were prepared with an internal pressure near 1 atmosphere, which minimizes effects due to differential permeation of Ar and N_2 through the O-rings seals on the stopcocks.

Although we would have liked to conduct more sensitive storage tests, we have been hampered in this goal by difficulties in preparing flasks with sufficiently reproducible Ar/N_2 ratios with the above procedures. On fourteen separate dates, we purged sets of flasks (typically 4 in number) using the same approach as for the storage test, and then analyzed the flasks within a few days of preparation. The analyzed Ar/N_2 ratios of these flasks were 9 per meg higher than the purge tank on average, with a standard deviation of ±19 per meg. The deviations were not random. Flasks purged at the same time tended to cluster together with standard deviations relative to the replicate mean of around 8 per meg. Much of the overall flask variability was therefore evidently caused by changes in the Ar/N_2 ratio of the purge gas stream. Different purge flows, ranging from 0.5 to 4 STP l min^{-1} were used on different dates. The highest Ar/N_2 ratios were obtained under the highest flows, while lower flows tended to correlate with lower

Ar/N_2, although the variability was higher at lower flows. After the first few sets, we modified the purge setup to insulate the purged flasks from fluctuations in room temperature. This had no noticeable effect on the mean or variability of the Ar/N_2 content of the flasks. The deviations in Ar/N_2 from the purge gas were correlated with the deviations in O_2/N_2 with a slope of around 2:1 ($\delta(Ar/N_2):\delta(O_2/N_2)$), consistent with the ratio expected from thermal fractionation within high-pressure cylinders.

4. MODELED Ar/N_2 VARIATIONS

Before discussing flask results, we describe a numerical model used to simulate variations in atmospheric Ar/N_2 which is useful for comparing against the data. The model is based on the TM2 atmospheric tracer transport model (Heimann, 1995), with air-sea N_2 and Ar fluxes as a lower boundary condition. The air-sea N_2 flux was computed via Eq. (1) on a monthly basis over the ice-free ocean surface. The solubility derivatives needed in Eq. (1) were based on the Weiss (1970) solubility relation evaluated at the annual-mean sea-surface temperature (SST) at each grid point, and were treated as spatially variable but constant with time. The annual-mean SSTs and the ice mask were derived from the Shea et al. (1992) climatology. The heat fluxes needed in Eq. (1) were treated as separate annual-mean and monthly-anomaly components. The annual-mean component was based on the climatology of da Silva et al. (1994), while the monthly anomalies were based on the European Centre for Medium-Range Weather Forecasting (ECMWF) monthly heat flux climatology (Gibson et al., 1997). The air-sea Ar flux was computed by multiplying the N_2 flux by a constant scale factor of 0.0295. According to the solubility relations of Weiss (1970), this factor should vary slightly

with temperature, but the variations are too small to be significant. The model was run for a total of four years, using only the final model year for comparison with observations.

From the favorable data/model comparison presented in Battle et al. (2003), we are encouraged to believe that this model provides a reasonable "first guess" for the mean annual cycle of atmospheric Ar/N_2 ratio, with a probable phasing error of order 1 month. Although we cannot be as confident in the predicted annual-mean Ar/N_2 values, the model still should be useful for establishing the plausible rough magnitude of annual-mean gradients.

5. FLASK RESULTS

5.1 Station data

Results for Ar/N_2 from flasks collected at an array of 9 stations are presented in Figure 11 as summarized in Tables 4 and 5. The data are collapsed into a single year since the data do not resolve any meaningful long-term trends.

Also shown in Figure 11 are the model simulations of the expected seasonal variations in Ar/N_2. The model output for the grid points corresponding to the flask sampling stations were fit to a function consisting of a constant (annual-mean value) plus an annual cycle (consisting of the fundamental plus 3 harmonics). To facilitate graphical comparison of the model and observations, we adjust the model predictions at each station by an additive constant to minimize the residuals between the model and the individual flask concentrations in a least squares sense. The annual-mean value of the adjusted model is therefore effectively a measure of the observed, rather than modeled, annual-mean Ar/N_2 at each station. These adjusted annual-means are summarized in Table 5 along with the annual-mean concentrations originally predicted by the

model.

The observed annual-mean values all lie within a range of -6 to +2 per meg, except for the result from the South Pole, which lies at +10 per meg. These annual-means are not highly sensitive to the method of computation. For example, repeating the fitting procedure with no cycle or with a cycle double in amplitude changes the estimated mean values by only a few per meg. Although the differences in annual-mean values between stations are statistically robust in some cases, we nevertheless are inclined to view these differences as being mostly the result of systematic sampling errors. Using similar sampling procedures, Battle et al (2003) report gradients as large as 30 per meg between stations in their network. Although we see no evidence of such large artifacts in our data averages, it is clear that improvements in methodology will be needed before gradients as small as those expected from the model simulation can be resolved with confidence.

Due to the large scatter and the limited number of samples collected to date, our data are only marginally able to resolve seasonal cycles, although they do provide bounds on the possible magnitude of the cycles. To provide a quantitative model/data comparison, we bin the individual flask measurements into two three-month seasons, Aug.-Oct. and Feb. -Apr., and compare the mean concentrations for these periods. These seasons were selected, a priori, to coincide roughly with the expected maxima and minima in the Ar/N_2 cycles. We also average the model output over similar three-month periods, using periods shifted one month earlier to account for the expected phasing error. The modeled and observed seasonal differences are compared in Table 5. The stations with the best resolved seasonal differences are Cold Bay, La Jolla, and Palmer, where seasonal differences of the order of 10 to 20 per meg are evident, in agreement

with model predictions. The most notable discrepancy is at Alert, where the data seem to indicate a cycle with opposite phasing from the model. A similar discrepancy may exist at Mauna Loa. At the South Pole, where three years of data are available, a cycle is evident in the data, but shifted several months later than the model predictions. At the remaining stations (Kumukahi, Samoa, and Cape Grim), the observed seasonal differences are marginally significant, with a sign and rough magnitude that agrees with the model predictions.

The standard deviation of the residuals in Figure 11, between observations and the model are given in Table 5. Depending on the station, these standard deviations, which we denote as $\sigma_{overall}$, range from ±11 to ±23 per meg. These standard deviations are not sensitive to the details of the model. For example, repeating the fitting procedure with no cycle or with a cycle doubled in amplitude changes the resulting standard deviations by typically 20% or less.

5.2 Discussion of Noise Sources

In this section we discuss the possible origins of the overall scatter in our data as reflected in the parameter $\sigma_{overall}$. We start by dividing $\sigma_{overall}$ into two contributions according to

$$\sigma_{overall}^2 = \sigma_{corr}^2 + \sigma_{uncor}^2$$

where σ_{uncor} is the 1 sigma error based on flask replicates, as described earlier. This separation, carried out station-by-station, is summarized in Table 5. It is seen that σ_{uncor} and σ_{corr} are of comparable magnitude and thus make comparable contributions to the overall scatter. There are some notable differences between stations, with ALT and SPO having both larger correlated and

uncorrelated errors relative to other stations.

5.2.1 Uncorrelated errors

The uncorrelated error σ_{uncor} can arise from three potential sources: (1) noise in the mass spectrometer, (2) errors in the daily working gas determinations, or (3) random variability in the air recovered from the flasks. The mass spectrometer contributes around ±3 per meg, based on the allowed integration time of 4 minutes on the flask peak and 4 minutes for each leading and trailing baseline (see Figure 9) and based on the 10-second imprecision in δ_i of ±10 per meg. The working gas contributes at most around ±2 per meg, based on the results from Figure 7. Taking the quadrature sum of these two contributions yields only ±4 per meg, which is essentially negligible compared to the observed total σ_{uncor} of (typically) ±11 per meg. We conclude, therefore, that the third source must dominate - in other words, that almost all of the scatter among replicates arises from actual variations in the Ar/N_2 ratios of the air recovered from the flasks.

The variability in the air recovered from flasks could arise either from gas handling in laboratory or in the field. Although we cannot clearly separate these two contributions, a substantial contribution almost certainly arises from laboratory practices. A laboratory imprecision of around ±8 per meg would be consistent with the results from baseline tests, described above. Also supporting a laboratory contribution are results we obtained using a different laboratory setup, which we employed briefly in 1998. Excluding flasks collected from the South Pole, this setup achieved an uncorrelated imprecision of ±4 per meg in Ar/N_2 (based on 77 flasks), which is considerably better than we achieve with our present setup. In this

temporary setup, which was permanently disassembled when relocating the lab in early 1999, flask air was delivered to the mass spectrometer via a pickoff T located directly upstream of the interferometer (see Figure 1 of Keeling et al. (1998)). This allowed higher flows (~260 STP mL min^{-1}) to be maintained through the flasks during analysis, while eliminating the pressure drop during analysis, which was possibly advantageous in reducing fractionation in the laboratory.

A substantial contribution to the random variability of the air recovered from flasks probably also arises from flask handling outside our laboratory, either during the sampling, shipping, or storage of flasks. Station-specific effects are implicated at several stations, e.g. Alert, Palmer Station, and the South Pole, where the uncorrelated error appears larger than at other stations. Larger uncorrelated error was also noted at the South Pole in flasks analyzed with the temporary setup used in 1999.

As noted earlier, the observed correlation of 4:1 between the Ar/N_2 and O_2/N_2 residuals (Figure 10b) is consistent with the ratio expected from thermal diffusion at 1 atm pressure. Thermal diffusion could occur either in the field and laboratory. For example, in the laboratory, the effect could arise from residual temperature gradients around the flasks during analysis or from flask-to-flask variability in the pressure-induced thermal fractionation, described in section 3.3. In the field, variable thermal fractionation could occur at the sampling intake, e.g. due to solar heating, or in the flasks themselves, due to non-uniform temperatures during sampling. It should be noted, however, that thermal fractionation is unlikely to be the sole cause of replicate variability, because many of the points in Figure 10b lie well off the 4:1 line. Among the possible complications are oxidation reactions that influence only O_2 and O-ring effects.

5.2.2 Correlated Errors

Turning now to the correlated errors, which are shared by all members of flask replicates, we can conceive of four possible contributions: (1) real atmospheric variability that is not reflected in the smoothed model results, e.g. related to the passage of synoptic weather patterns, (2) other natural atmospheric variability, (3) sampling artifacts, and (4) storage effects. We now discuss these possibilities in turn.

An estimate of the contribution from synoptic variability can be formulated based on a scaling argument that makes use of the observed variability in O_2/N_2 ratio and CO_2 concentration. As described in Stephens et al. (1998), it is possible to combine O_2/N_2 ratio and CO_2 data to derive the tracer "APO", that undergoes seasonal cycles and synoptic variability as a consequence primarily of air-sea exchanges of O_2. The seasonal air-sea fluxes of O_2, although partially biologically mediated, are largely controlled by ocean heating and cooling (Garcia and Keeling, 2001), and thus should be strongly correlated with air-sea Ar and N_2 fluxes. Given that the surface sources of APO and Ar/N_2 are highly correlated, the synoptic variability in Ar/N_2 must be similar in magnitude to the synoptic variability in APO, when both are expressed as a fraction of the seasonal cycle. Since we have observations of the variability in APO at each of our stations, we can thus easily formulate an estimate of the expected synoptic variability in Ar/N_2 at each station. As summarized in Table 5, the estimates vary between ±2.5 and ±5 per meg, depending on the station. These estimates assume that the Ar/N_2 cycle at each station has a magnitude equal to 30% of the corresponding APO cycle (with both expressed in per meg units), which is roughly consistent with the Ar/N_2 model predictions in relation to our APO observations and consistent with the results presented in Battle et al. (2003). These estimates of

Ar/N_2 variability probably should be treated as upper bounds, since the scatter in our APO data, which we use as a measure of synoptic variability, may also partly be due to measurement artifacts. In any case, it is clear that synoptic variability makes a negligible contribution to the scatter in our Ar/N_2 data.

While synoptic variability may not be a major contributor to the correlated errors, another source of natural variability perhaps deserves attention. Throughout the free troposphere the separation of air into its constituent components by gravimetric or thermal diffusive separation is overwhelmed by turbulent mixing. However, it is conceivable that within stable surface air layers that are capped by strong inversions, a slight separation may occur. In the absence of turbulent motions, Ar/N_2 would fractionate by ~52 per meg per meter of elevation at 0EC or by ~260 per meg per degree Celcius in a thermal gradient.

Consider, for example, a surface layer 30m thick with a 5EC gradient from top to bottom and which maintains a constant composition at the top by turbulent mixing with air above. First, suppose the air within the layer is completely stagnant. The air at the surface will be enriched in Ar/N_2 by 3200 per meg relative to the overlying air, with 60% of the enrichment due to gravimetric fractionation and 40% due to thermal fractionation. At 15m the enrichment would be half that large, i.e. 1600 per meg, etc. The time scale for approaching this steady-state is ~265 days, based on the molecular diffusivity of Ar in air at 0EC of D_{mol}=0.16 cm^2 sec^{-1}(Reid et al., 1987). Now suppose that the air within the layer is not stagnant, but rather is exchanged with the overlying air on a time scale of one day. This corresponds to an effective eddy diffusivity within the layer of around D_{eddy} = 42 cm^2 $sec^{-1.}$ In steady-state, the enrichment is now 12 per meg at the surface and 6 per meg at 15m, while the time scale for approaching steady-state is ~1 day. The

enrichment and the time-scale for approaching steady-state are both smaller than the stagnant case by a factor of $D_{mol}/(D_{eddy}+D_{mol})$. The calculation shows that measurable enrichment may occur within surface layers with depths of order of ten meters if the exchange times are a long as tens of hours. The calculation does not consider the effects of convergent subsidence flow, which could lead to excess Ar accumulation into even deeper layers.

Most of our samples are collected in daylight in the absence of strong inversions, so are unlikely to be influenced by this sort of mechanism. At Alert and the South Pole Stations, however, strong inversions are present throughout the winter (Kahl et al., 1992; Neff, 1999). The near-surface residence time of air at these sites is not well constrained but is almost certainly of the order of hours or more. It is thus conceivable that measurable near-surface fractionation is occurring. The effects could potentially bias both the mean values and annual cycles at these stations relative to the background troposphere.

Another possible source of correlated error is fractionation at the air intake in the field. Using a continuous field-based O_2/N_2 system with a sampling rate of 100 STP mL min^{-1}, Manning (2001) noted swings of order 20 to 30 per meg in O_2/N_2 over an hourly time scale which he attributed to thermal diffusion at the intake (e.g. related to solar heating), and which therefore were presumably associated with swings in Ar/N_2 that were ~4 time larger. Manning reduced the effect by removing a glass-wool filled PVC pipe used as a particle filter from the intake, which reduced the residence time of air in the inlet. A similar effect may influence our flask results, although the magnitude of the effect will be many times smaller due to the much larger sampling flows we employ (2 to 5 L min^{-1}). Thermal diffusion at the intake can presumably be reduced by increasing the sampling flow (e.g. using larger pumps). Shading of

the intake from sunlight and restricting sampling to periods of higher winds may also be helpful.

Finally, we must consider the possibility that correlated errors could arise from storage effects. Although we do not expect significant systematic storage effects at most of our stations on the basis of the storage tests reported above, these test do not rule out substantial problems at the South Pole, where the flasks are stored at the station for as much as nine months before return shipment. As the station pressure is typically 680mb, we might expect our South Pole flasks to be influenced by permeation through the stopcock O-rings to a much greater extent than flasks used in our storage tests. Any such effect, however, would be expected to produce a discontinuity in the South Pole data in late December, since storage times are much greater for flasks after this time of year than before. (The storage times at the South Pole vary depending on the time of year as dictated by the inaccessibility of the station during colder months. The storage times at the station are typically 9 months for samples collected in January, 8 months for samples collected in February, etc., and decreasing to two months or less for samples collected between October and December.) Since our results show no obvious discontinuity in late December, (see Figure 11), we conclude that storage effects are unlikely to be a major contributor to the correlated error at the South Pole, although we cannot rule out a small contribution. Storage effects cannot account, for example, for the apparent rise in Ar/N_2 from January through March at the South Pole and the subsequent fall through the remainder of the calendar year.

6. SUMMARY

We have described a mass spectrometer system developed to resolve variations in atmospheric Ar/N_2, O_2/N_2 and CO_2/N_2 ratios. The system takes advantage of the evolving

technology in wide-dispersion mass spectrometers and uses a rapid switching scheme to cancel instrument noise on longer time scales, thus increasing instrument precision. The system allows two flowing gas streams to be compared to a precision of around 10 per meg in Ar/N_2 every 10 seconds, and also allows simultaneous measurement of CO_2/N_2 and O_2/N_2 ratios to very high precision. The Ar/N_2 signals can be meaningfully averaged to compare Ar/N_2 ratios from air delivered from high pressure cylinders to a precision of a few per meg. These results demonstrate that considerable progress is being made technology for measuring changes in the Ar/N_2 ratio of the atmosphere and provide a basis for optimism that such measurements may eventually prove useful for improving estimates of large-scale air-sea heat transport.

The system has been applied to analyze flask samples from a global network of stations. Marginally significant seasonal cycles have been resolved at several stations. The data show surprisingly large scatter, however, which limits their usefulness. This scatter arises mostly from real variations in the Ar/N_2 ratios in the air extracted from the flasks. These variations are evidently caused by gas handling artifacts in both the laboratory and in the field. We see clear evidence of variations that are uncorrelated among sets of flask replicates, and hence may average to zero, as well as errors that, more troublingly, are correlated among sets of flask replicates. In the absence of a clear understanding of these effects, we must assume that these errors have the potential to bias both the seasonal cycles and annual-mean values obtained at different stations. Although similar problems undoubtedly also impact O_2/N_2 measurements made on the same flasks, the effects tend to be smaller for O_2/N_2 by a factor between 2 and 4.

The mass spectrometer system described here provides a powerful tool for diagnosis of possible fractionation mechanism due to its high intrinsic precision, so we are optimistic that

substantial improvements in flask handling can be realized in the future. These efforts can be expected to also improve the quality of O_2/N_2 measurements. Furthermore, a shorter path to making precise atmospheric Ar/N_2 may be possible by using mass spectrometer systems, like that described here, for direct field measurements, bypassing the need for flasks altogether. The ISOPRIME is especially attractive for this purpose, due to is reliability (< 2 filaments needed per year of operation) and its low size and weight.

ACKNOWLEDGMENTS

We are indebted to Michael Bender and Mark Battle for useful discussions. This work was supported by the U.S. NSF under grants ATM-940000694, ATM-9601722, ATM-0000923, and NOAA Office of Global Programs under grant NA77RJ0453A. T. Blaine was supported by a U.S. National Defense Science and Engineering Graduate Fellowship. Much of this work was completed in part while one of us (R.K.) was hosted at the Max Planck Insitute for Biogeochemistry in Jena, Germany. We thank the staff of the NOAA-CMDL program at Mauna Loa, Kumukahi, Samoa, and the South Pole, staff of the National Weather Service at Cold Bay, staff of the Cape Grim Station, and staff of Palmer Station, for collection of air samples.

REFERENCES

Baggeroer A. B., Birdsall T. G., Clark C., Colosi J. A., Cornuelle B. D., Costa D., Dushaw B. D., Dzieciuch M., Forbes A. M. G., Hill C., Howe B. M., Marshall J., Menemenlis D., Mercer J. A., Metzger K., Munk W., Spindel R. C., Stammer D., Worcester P. F. and Wunsch C., 1998. Ocean climate change: Comparison of acoustic tomography, satellite altimetry, and modeling. *Science* **281**(5381), 1327-1332.

Battle M., Bender M., Hendricks M. B., Ho D. T., Mika R., McKinley G., Fan S.-M., Blaine T. and Keeling R. F., 2003. Measurements and models of the atmospheric Ar/N_2 ratio. *Geophysical Research Letters* **30**(15), art no. 1786.

Bender M. L., Tans P. P., Ellis J. T., Orchardo J. and Habfast K., 1994. A High-Precision Isotope Ratio Mass-Spectrometry Method for Measuring the O_2/N_2 Ratio of Air. *Geochimica Et Cosmochimica Acta* **58**(21), 4751-4758.

Cabanes C., Cazenave A. and Le Provost C., 2001. Sea level rise during past 40 years determined from satellite and in situ observations. *Science* **294**(5543), 840-842.

Craig H., Weiss R. F. and Clarke W. B., 1967. Dissolved gases in the Equatorial and South Pacific Ocean. *Journal of Geophysical Research* **72**, 6165-6181.

Craig H. and Wiens R. C., 1996. Gravitational enrichment of Kr-84/Ar-36 ratios in polar ice caps: A measure of firn thickness and accumulation temperature. *Science* **271**(5256), 1708-1710.

Da Silva A. M., Young C. and Levitus S., 1994. *Atlas of surface marine data 1994 Volume 1: Algorithms and procedures. NOAA Atlas NESDIS 6*.

Garcia H. E. and Keeling R. F., 2001. On the global oxygen anomaly and air-sea flux. *Journal of*

Geophysical Research - Oceans **106**(NC12), 31155-31166.

Gibson J. K., Kållberg P., Uppala S., Hernandez A., Nomura A. and Serrano E., 1997. *ERA description*. Eur. Cent. for Medium-Range Weather Forecasts.

Gille S. T., 2002. Warming of the Southern Ocean since the 1950s. *Science* **295**(5558), 1275-1277.

Glueckauf E. (1951) The composition of atmospheric air. In *Compendium of Meteorology* (ed. T. Malone), pp. 3-10. American Meteorological Society.

Grew K. E. and Ibbs T. L., 1952. *Thermal diffusion in gases*. Cambridge University Press.

Hamme R. C. and Emerson S. R., 2002. Mechanisms controlling the global oceanic distribution of the inert gases argon, nitrogen and neon. *Geophysical Research Letters* **29**(23), art. no. 2120.

Heimann M., 1995. *The global atmospheric tracer model TM2*. Deutsches Klimarechenzentrum.

Kahl J. D., Serreze M. C. and Schnell R. C., 1992. Tropospheric low-level temperature inversions in the Canadian Arctic. *Atmos. Ocean* **30**(4), 511-529.

Keeling R. F., Najjar R. P., Bender M. L. and Tans P. P., 1993. What atmospheric oxygen measurements can tell us about the global carbon-cycle. *Global Biogeochemical Cycles* **7**(1), 37-67.

Keeling R. F., Manning A. C., McEvoy E. M. and Shertz S. R., 1998. Methods for measuring changes in atmospheric O_2 concentration and their application in southern hemisphere air. *Journal of Geophysical Research-Atmospheres* **103**(D3), 3381-3397.

Leuenberger M., Nyfeler P., Moret H. P., Sturm P. and Huber C., 2000. A new gas inlet system for an isotope ratio mass spectrometer improves reproducibility. *Rapid Communications*

in Mass Spectrometry **14**(16), 1543-1551.

Levitus S., Antonov J. I., Boyer T. P. and Stephens C., 2000. Warming of the world ocean. *Science* **287**(5461), 2225-2229.

Levitus S., Antonov J. I., Wang J. L., Delworth T. L., Dixon K. W. and Broccoli A. J., 2001. Anthropogenic warming of Earth's climate system. *Science* **292**(5515), 267-270.

Manning A. C., 2001. Temporal variability of atmospheric oxygen from both continuous measurements and a flask sampling network: tools for studying the global carbon cycle, Ph. D. Thesis University of California, San Diego.

Munk W. and Wunsch C., 1979. Ocean Acoustic Tomography - Scheme for Large-Scale Monitoring. *Deep-Sea Research Part a-Oceanographic Research Papers* **26**(2), 123-161.

Neff W. D., 1999. Decadal time scale trends and variability in the tropospheric circulation over the South Pole. *Journal of Geophysical Research-Atmospheres* **104**(D22), 27217-27251.

Ozima M. and Podosek F. A., 1983. *Noble gas geochemistry*. Cambridge University Press.

Peixoto J. P. and Oort A. H., 1992. *Physics of Climate*. American Institute of Physics.

Reid R. C., Prausnitz J. M. and Poling B. E., 1987. *The Properties of Gases and Liquids, 4th Edition*. McGraw-Hill.

Samuels B. L. and Cox M., 1987. Date set atlas for oceanographic modeling. *Ocean Modeling* **75**, 1-3.

Schudlich R. and Emerson S., 1996. Gas supersaturation in the surface ocean: The roles of heat flux, gas exchange, and bubbles. *Deep-Sea Research Part Ii-Topical Studies in Oceanography* **43**(2-3), 569-589.

Severinghaus J. P., Grachev A. and Battle M., 2001. Thermal fractionation of air in polar firn by

seasonal temperature gradients. *Geochemistry Geophysics Geosystems* **2**, art. no.-2000GC000146.

Shea D. J., Trenberth K. E. and Reynolds R. W., 1992. A global monthly sea surface temperature climatology. *Journal of Climate* **5**, 987-1001.

Spitzer W. S. and Jenkins W. J., 1989. Rates of vertical mixing, gas exchange, and new production: estimates from seasonal gas cycles in the upper ocean near Bermuda. *Journal of Marine Research* **47**, 169-196.

Stephens B. B., Keeling R. F., Heimann M., Six K. D., Murnane R. and Caldeira K., 1998. Testing global ocean carbon cycle models using measurements of atmospheric O_2 and CO_2 concentration. *Global Biogeochemical Cycles* **12**(2), 213-230.

Stute M., Forster M., Frischkorn H., Serejo A., Clark J. F., Schlosser P., Broecker W. S. and Bonani G., 1995. Cooling of Tropical Brazil (5-Degrees-C) During the Last Glacial Maximum. *Science* **269**(5222), 379-383.

Tans P. P., Conway T. J. and Nakazawa T., 1989. Latitudinal distribution of the source and sinks of atmospheric carbon dioxide derived from surface observations and an atmospheric transport model. *Journal of Geophysical Research* **94**, 5151-5173.

Trenberth K. E., 1981. Seasonal variations in global sea level pressure and the total mass of the atmosphere. *Journal of Geophysical Research* **86**(C6), 5238-5246.

Trengove R. D. and Dunlop P. J., 1982. Diffusion coefficients and thermal diffusion factors for five binary systems of nitrogen and a nobel gas. *Physica* **115A**, 339-352.

Weiss R. F., 1970. Solubility of nitrogen, oxygen, and argon in water and seawater. *Deep-Sea Research* **17**, 721-735.

Table 1. Effect of ocean warming at different temperatures on global atmospheric composition

	Mole fraction in dry air[†]	Relative change in atmospheric burden[§], $(dP_i/P_i)\times10^6$, per 100 ZJ of ocean warming		
		0EC	10EC	20EC
He	5.24×10^{-6}	0.23	0.14	0.10
Ne	$18.2\times10^{!6}$	0.54	0.40	0.33
N_2	0.0781	2.66	1.75	1.22
Ar	0.00934	6.56	4.31	2.99
Kr	$1.14\times10^{!6}$	16.40	10.43	6.95
Xe	$0.087\times10^{!6}$	40.27	23.73	14.80

[†]Glueckauf (1951).

[§]Computed from Eq. (1) based on the total mass of dry air of 5.124×10^{21}g (Trenberth, 1981), a mean molecular weight of dry air of 28.97g $mol^{!1}$, and solubility data compiled in Ozima and Podosek (1983) for a salinity of 35 PSU.

Table 2. Mass spectrometer detector configuration

Collector (M/Z)	Feedback Resistance (G Ω)	Typical Ion Current (nA)	Typical Amplifier Voltage (V)
28	0.1	37	3.7
29	20	0.27	5.4
30	1†	0.15	1.5
32	0.5	8.6	4.3
34	200	0.036	7.2
36	2†	0.059	0.12
40	5	0.78	3.6
44	200	0.028	5.6

†Resistance sized for isotope dilution studies

Table 3. Thermal Diffusion factors for Ar/N_2 and O_2/N_2 in air

Description	Magnitude	References*
α_T for Ar/N_2 at 1 atm, 20EC	0.071	(1)
α_T for Ar/N_2 at 1 atm, 27EC	0.074	(2)
α_T for O_2/N_2 at 1 atm, 20EC	0.018	(1)
Ω for Ar/N_2 at 1 atm, 20EC	242 per meg EC[!1]	(1)
Ω for O_2/N_2 at 1 atm, 20EC	61 per meg EC[!1]	(1)
D for Ar in air at 1 atm, 20EC	0.19 $cm^3\ s^{-1}$	(3)
D for O_2 in air at 1 atm, 20EC	0.20 $cm^3\ s^{-1}$	(3)
$(\alpha_T D)_{(Ar/N2)}/(\alpha_T D)_{(O2/N2)}$ in air at 1 atm, 20EC	4.15	(1) & (3)
$(\alpha_T D)_{(Ar/N2)}/(\alpha_T D)_{(O2/N2)}$ in air at 1 atm, 20EC	3.77±0.04	this work
$(\alpha_T D)_{(Ar/N2)}/(\alpha_T D)_{(O2/N2)}$ in air at 120 atm, 20EC	2.17±0.02	this work

* (1) Grew and Ibbs(1952, p. 130); (2) Eq. (5) in Trengove and Dunlop (1982) using Ar mole fraction of $x_1 = 0.01$; (3) Formula of Fuller, as described in Reid et al., (1987, p. 587).

Table 4. Sampling stations in the Scripps flask network.

Station Code	Site	Lat.	Lon.	Elevation (m)	Time Period
ALT	Alert, Northwest Territories	82E27'N	62E31'W	210	Jul. 2001 - Nov. 2002
CBA	Cold Bay, Alaska	55E12'N	162E43'W	25	Jul. 2001 - Nov. 2002
LJO	La Jolla, California	32E52'N	117E15' W	20	Jun. 2001 - Jun. 2003
MLO	Mauna Loa, Hawaii	19E32'N	155E35'W	3397	Aug. 2001 - Dec. 2002
KUM	Kumukahi, Hawaii	19E31'N	154E49'W	40	Jul. 2001 - Dec. 2002
SMO	Cape Matatula, American Samoa	14E15'S	170E34'W	42	Aug. 2001- Dec. 2002
CGO	Cape Grim, Tasmania	40E41'S	144E41'E	94	Aug. 2001 - Dec. 2002
PSA	Palmer Station Antarctica	64E55'S	64E 0'W	10	May 2001- Nov. 2002
SPO	South Pole Station	89E59'S	24E48'W	2810	Jan. 2000 - Dec. 2002

Table 5. Ar/N_2 statistics from field stations (per meg)

	ALT	CBA	LJO	MLO	KUM	SMO	CGO	PSA	SPO
Modeled annual-mean‡	-4.7	-3.6	-2.9		-3.1	-1.3	0.0	0.6	0.0
Observed annual-mean‡	2±3	-2±2	-6±1	0±2	2±2	-4±2	0±3	-3±2	10±2
Modeled Seasonality*	-13.4	-15.7	-10.3	-5.3	-7.8	6.7	20.1	23.1	19.3
Observed seasonality§	19±6	-13±4	!10±3	6±4	!14±6	9±4	8±5	16±6	9±5
Residuals from seasonal model ($\sigma_{overall}$)	±23	±14	±16	±15	±11	±15	±13	±15	±22
Uncorrelated error (σ_{uncor})	±12	±10	±10	±11	±9	±10	±11	±12	±14
Correlated error (σ_{corr})	±18	±10	±13	±11	±7	±10	±6	±10	±17
Synoptic Variability, estimated upper bound (1σ)†	±2.9	±3.8	±4.6	±2.6	±3.7	±2.7	±2.9	±2.6	±2.6

‡Difference from value at CGO.

*Differences between three-month averages, Jan/Feb/Mar minus Jul/Aug/Sep.

†Calculated from the variability in APO at each station (see text).

§ Differences between three-month averages, Feb/Mar/Apr minus Aug/Sep/Oct. The observed seasonality is computed one month later than modeled seasonality to account for expected one-month phasing error of the model.

FIGURES

Figure 1. Isoprime ion optics.

Figure 2. Mass spectrometer inlet system.

Figure 3. Sample data from mass spectrometer system at 0.1s resolution. Shown is the ratio (R) of two collector currents (e.g. M/Z = 40 versus M/Z = 28) expressed as parts-per-million deviation from an initial ratio. During this sequence, sample and instrument reference gases are being switched at regular 5 second intervals. The quantity δ_i is computed according to $\delta_i = (R_{samp}/R_{ref} -1)\times 10^6$, where R_{ref} is based on the average of the leading and trailing segments reference-gas segments. The initial ratio R_0 is used here for plotting purposes only.

Figure 4. Precision of the mass spectrometer for a hypothetical 20-minute sample-reference integration as a function of switching rates between sample and reference gas (see text). The results shown are based on a 20-minute segment of raw (0.1s) data, during which a single gas was introduced into the mass spectrometer without switching the changeover valve.

Figure 5. Manifold system for introducing flask samples.

Figure 6. Sample data from the mass spectrometer system at 10-second resolution, expressed as δ_i (see Figure 2). The sequence shows the changing value of the difference between the sample and the instrument reference gas as the sample side alternately receives gas from various tanks

(WT, A, B) or flasks.

Figure 7. (a) Working gas concentrations of $\delta(Ar/N_2)$ as a function of the (approximate) fractional tank usage. For each tank the mean value of $\delta(Ar/N_2)$ was subtracted to allow the curves to be overlaid. Zero usage corresponds to approximately the fill pressure of ~14000 kPA (2100 PSIG) while full usage (1.0) corresponds to a residual pressure of approximately ~800 kPA (120 PSIG). (b) Scatter plot of $\delta(Ar/N_2)$ versus $\delta(O_2/N_2)$ for same working tanks as (a).

Figure 8. Mass-spectrometer signals for Ar/N_2 and O_2/N_2 ratios (reported as δ_i) of the air delivered from a 5l flask during controlled testing. Initially, both inlet and outlet stopcocks of the flask are open, and the flask is purged with air of constant composition at a constant pressure. The inlet stopcock is then closed. This stops the inlet flow while leaving the exit flow unchanged (due to active control). The change in composition after stopping the inlet flow is attributed to thermal fractionation driven by pressure-induced cooling within the flask (see text). Points are 10-second values of δ_i. Lines are time averages over the corresponding segments.

Figure 9. Mass-spectrometer signals for Ar/N_2 ratio, reported as $\delta_i(40/28)$, immediately before, after, and during a flask analysis. The data shown are derived by bin-averaging 520 separate flask analyses.

Figure 10. Top panel: Normal probability plot of Ar/N_2 residuals relative to replicate average. Bottom panel: Residuals in Ar/N_2 versus residuals in O_2/N_2. Residuals have been scaled

according to $(N/(N-1))^{1/2}$, where N is the number of replicates (see text).

Figure 11. Observed (points) and modeled (curves) variations in the atmospheric Ar/N_2 ratio. The model curves have been adjusted vertically, via an additive constant, to optimally fit the observations at each station. Data have been collapsed into a single year to form a climatology, which is then displayed over two years. For the South Pole, the dashed line separates flasks that "winter-over" (after line) from those that are more promptly return shipped (before line). Station details given in Table 4.

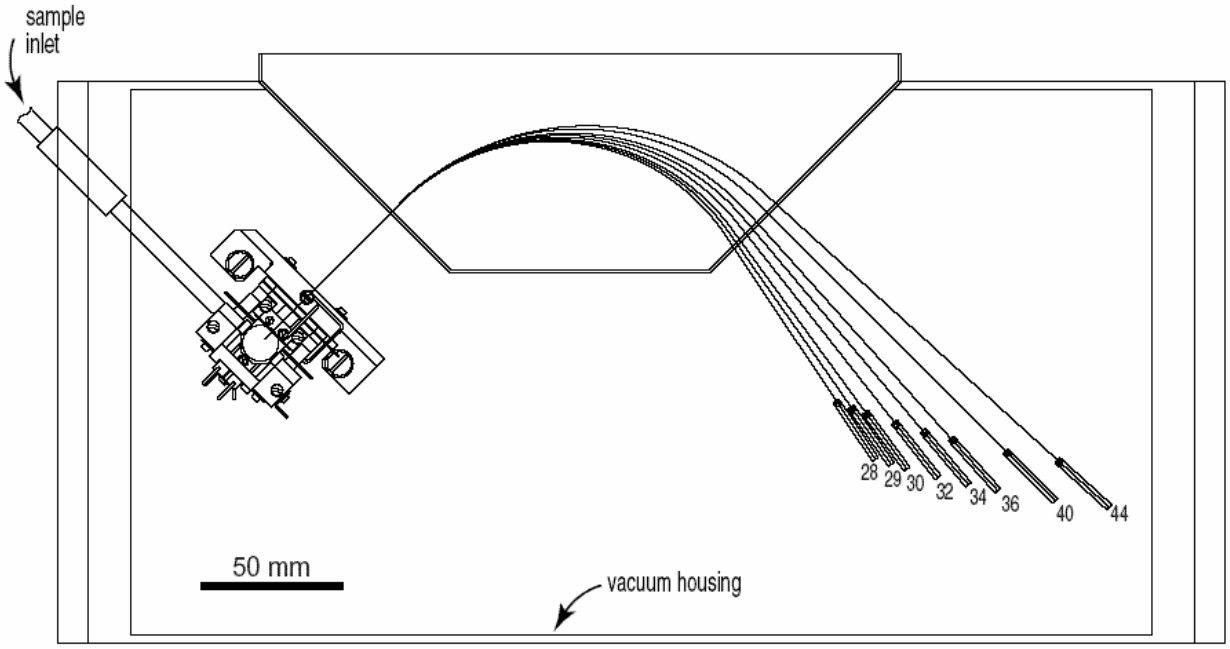

Figure 1.

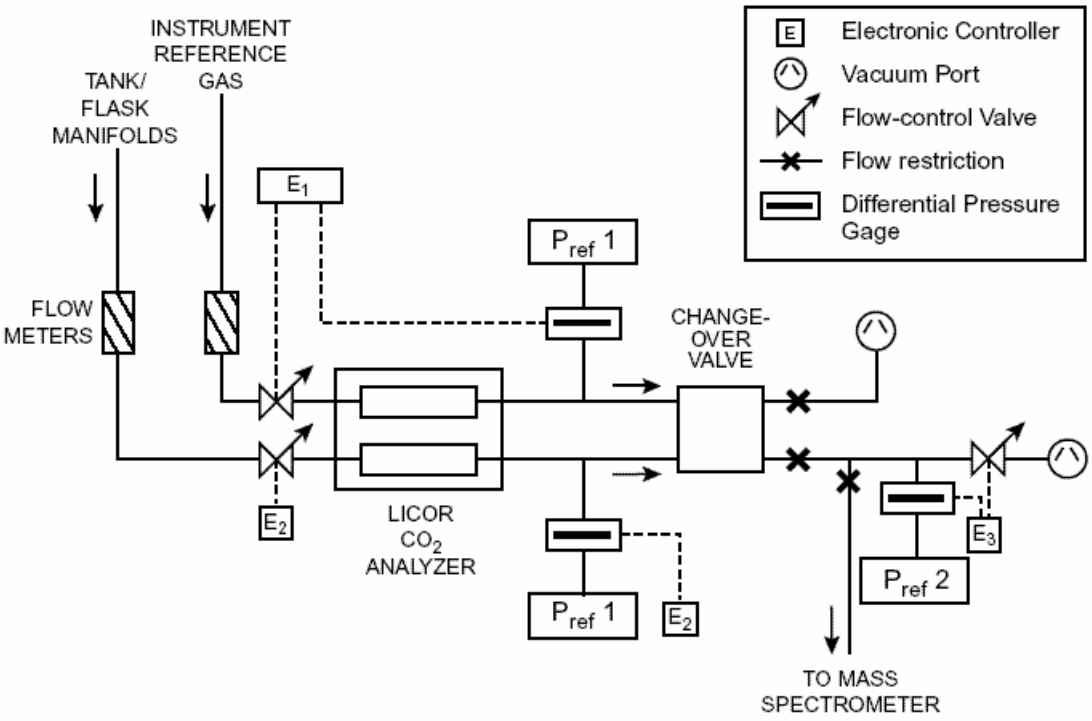
INSTRUMENT
REFERENCE
GAS
TANK/
FLASK
MANIFOLDS
FLOW
METERS
E1
Pref 1
CHANGE-
OVER
VALVE
E2
LICOR
CO2
ANALYZER
Pref 1
E2
E3
Pref 2
TO MASS
SPECTROMETER
E
Electronic Controller
Vacuum Port
Flow-control Valve
Flow restriction
Differential Pressure
Gage

Figure 2.

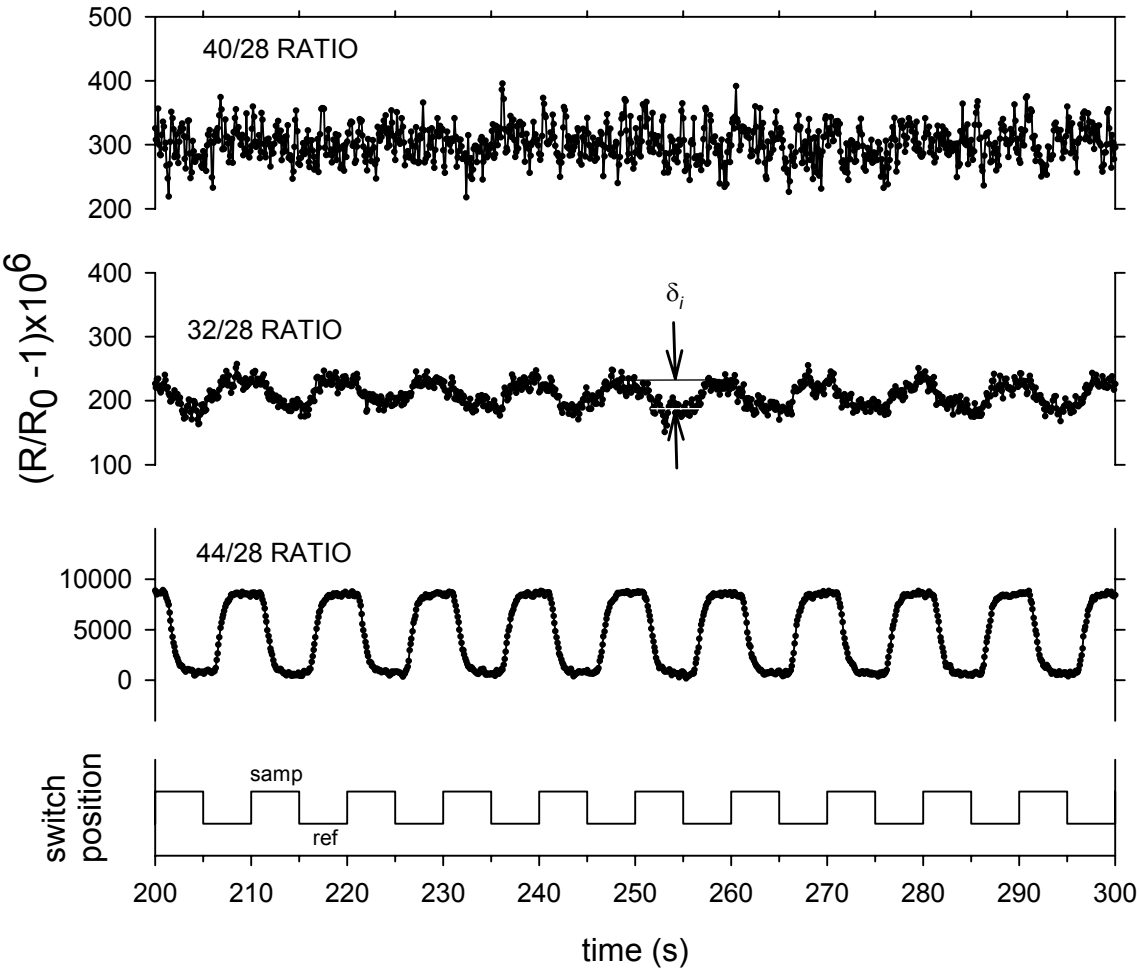
40/28 RATIO
32/28 RATIO
44/28 RATIO
δ_i
$(R/R_0 - 1)x10^6$
switch position
samp
ref
time (s)

Figure 3.

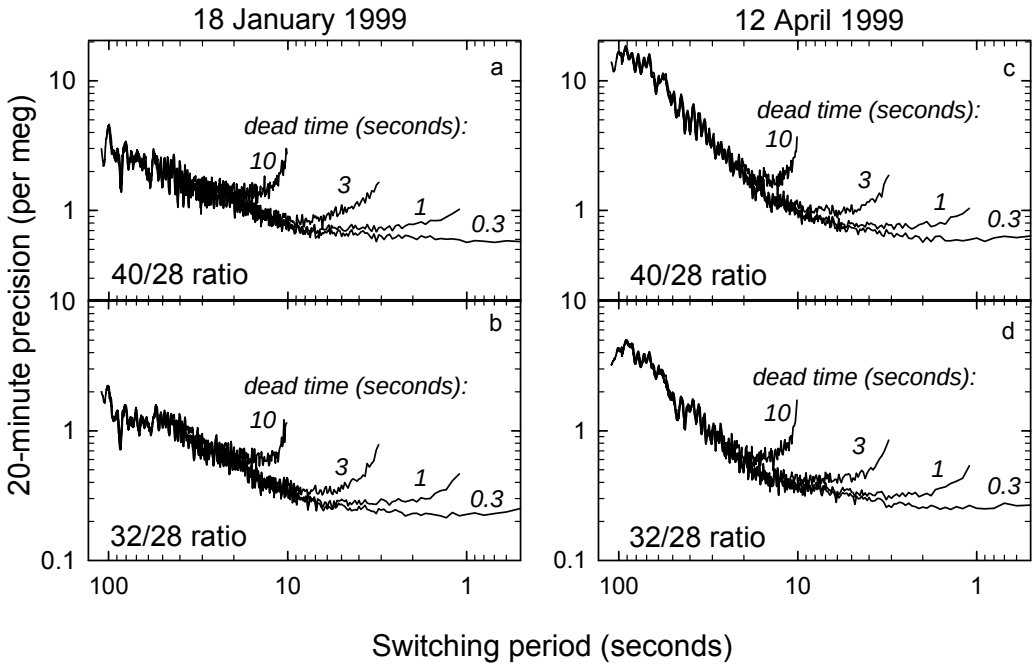
18 January 1999
12 April 1999
a
b
c
d
dead time (seconds):
10
3
1
0.3
40/28 ratio
32/28 ratio
20-minute precision (per meg)
Switching period (seconds)
10
1
0.1
100
10
1

Figure 4.

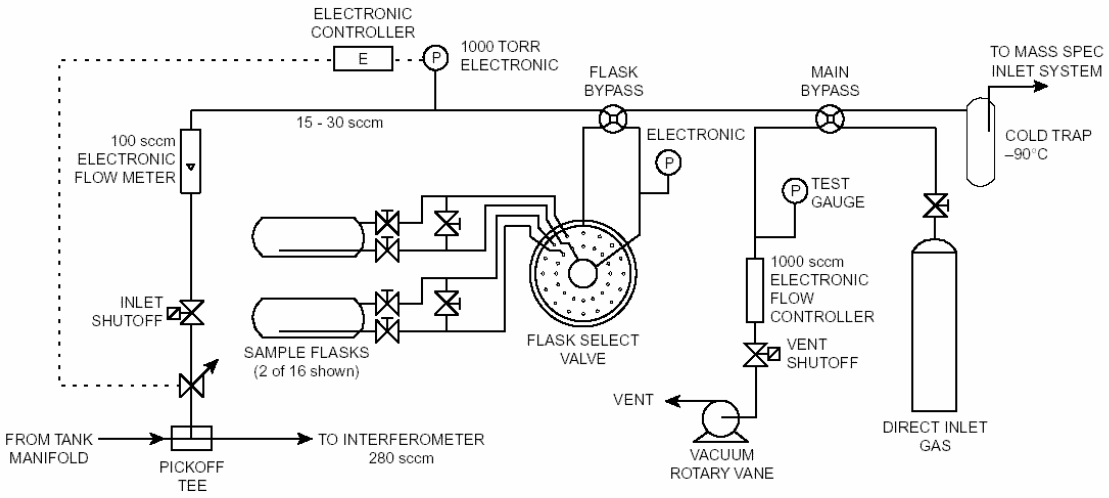
ELECTRONIC
CONTROLLER
E
P
1000 TORR
ELECTRONIC
FLASK
BYPASS
MAIN
BYPASS
TO MASS SPEC
INLET SYSTEM
15 - 30 sccm
100 sccm
ELECTRONIC
FLOW METER
ELECTRONIC
P
COLD TRAP
–90°C
P
TEST
GAUGE
1000 sccm
ELECTRONIC
FLOW
CONTROLLER
INLET
SHUTOFF
SAMPLE FLASKS
(2 of 16 shown)
FLASK SELECT
VALVE
VENT
SHUTOFF
VENT
FROM TANK
MANIFOLD
PICKOFF
TEE
TO INTERFEROMETER
280 sccm
VACUUM
ROTARY VANE
DIRECT INLET
GAS

Figure 5.

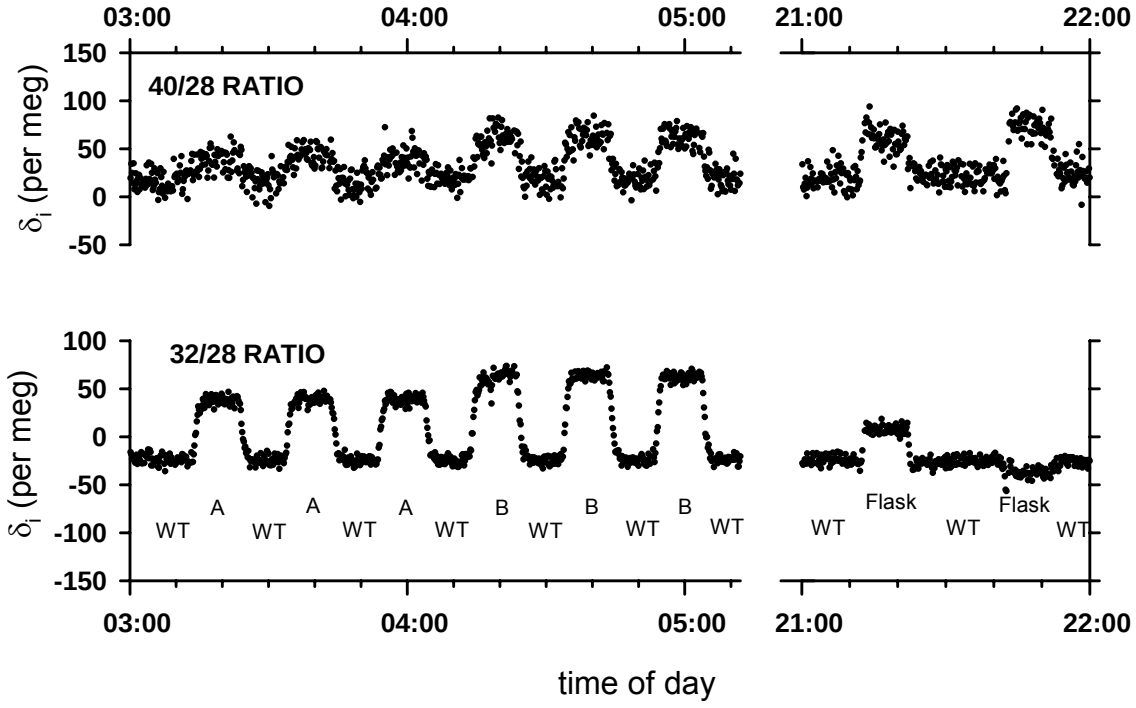
03:00
04:00
05:00
21:00
22:00
150
100
50
0
-50
40/28 RATIO
δi (per meg)
100
50
0
-50
-100
-150
32/28 RATIO
δi (per meg)
WT
A
WT
A
WT
A
WT
B
WT
B
WT
B
WT
WT
Flask
WT
Flask
WT
03:00
04:00
05:00
21:00
22:00
time of day

Figure 6.

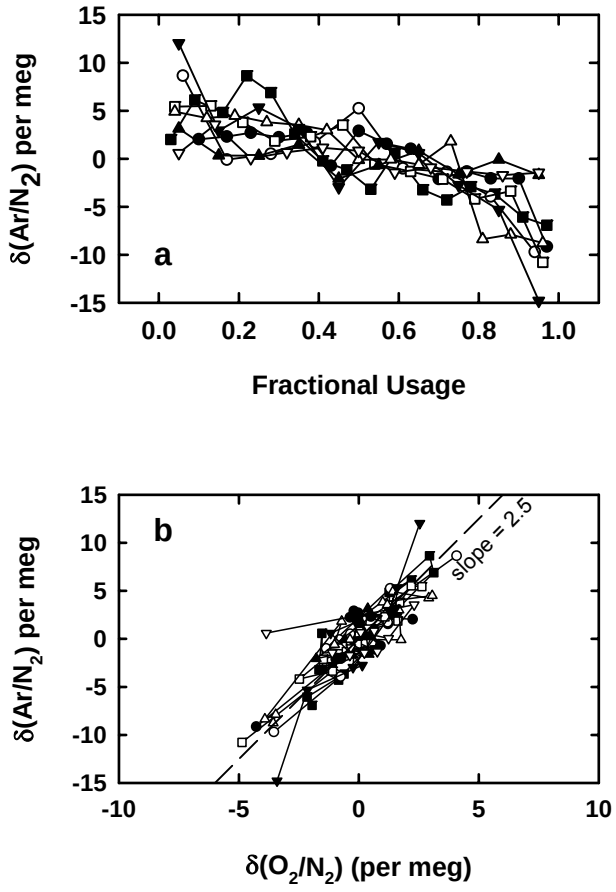
15
10
5
0
-5
-10
-15
δ(Ar/N2) per meg
a
0.0
0.2
0.4
0.6
0.8
1.0
Fractional Usage
b
slope = 2.5
-10
-5
0
5
10
δ(O2/N2) (per meg)

Figure 7.

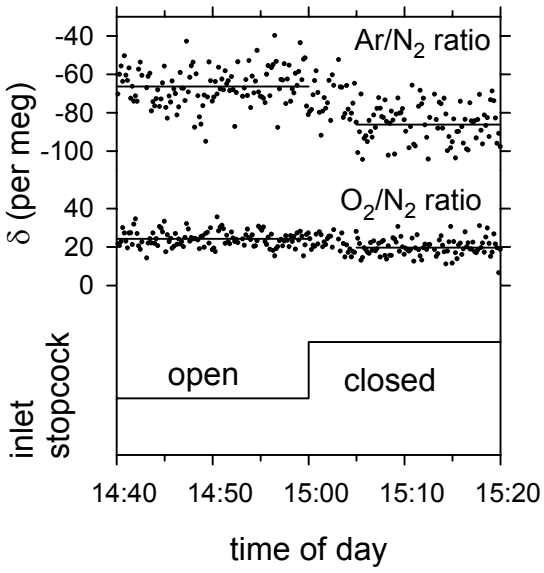
-40
-60
-80
-100
Ar/N2 ratio
δ (per meg)
40
20
0
O2/N2 ratio
inlet stopcock
open
closed
14:40
14:50
15:00
15:10
15:20
time of day

Figure 8.

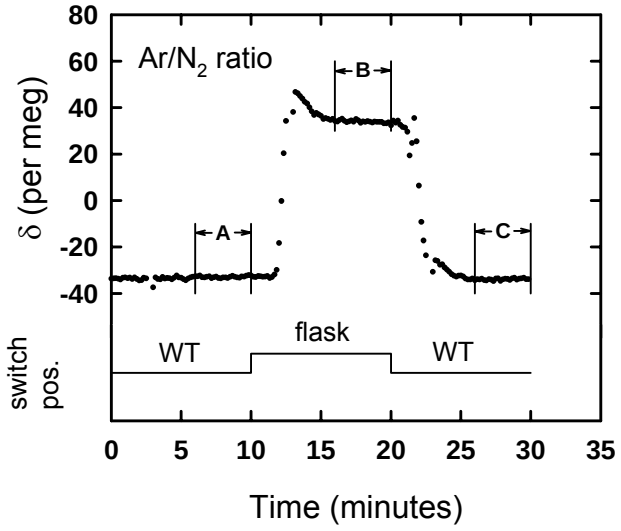
Ar/N2 ratio
δ (per meg)
80
60
40
20
0
-20
-40
A
B
C
flask
WT
WT
switch pos.
0
5
10
15
20
25
30
35
Time (minutes)

Figure 9.

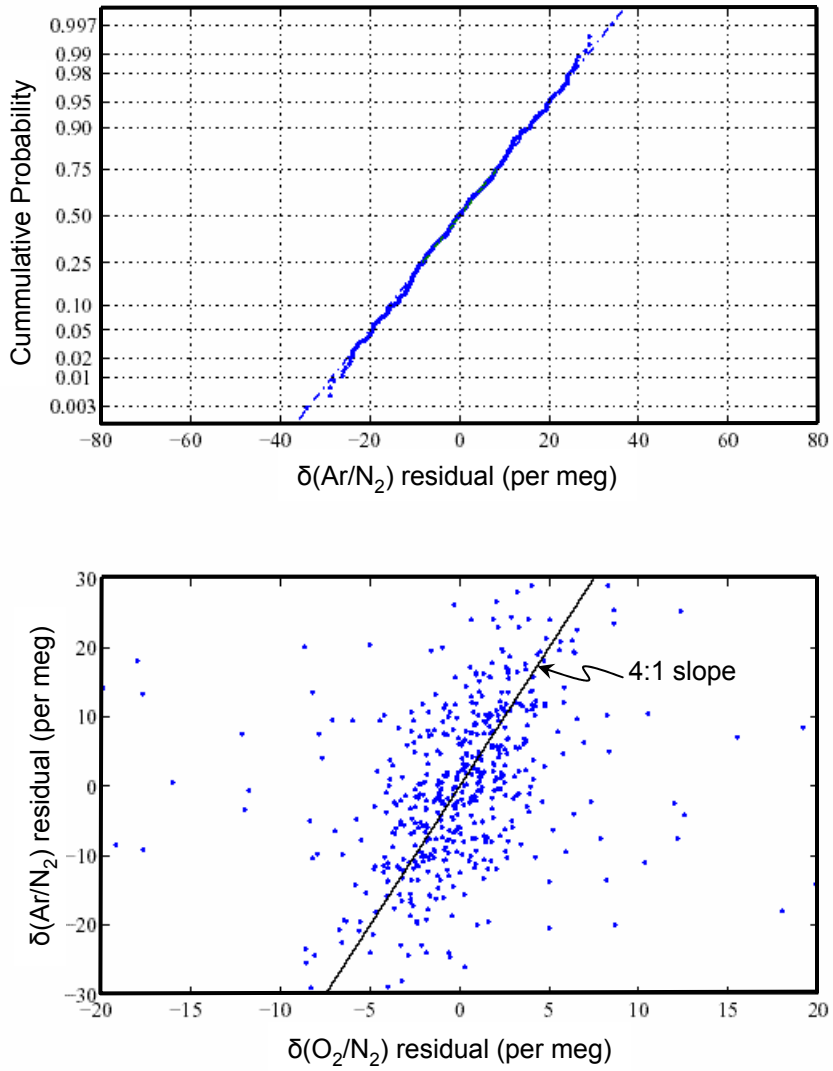
Cummulative Probability
0.997
0.99
0.98
0.95
0.90
0.75
0.50
0.25
0.10
0.05
0.02
0.01
0.003
−80
−60
−40
−20
0
20
40
60
80
δ(Ar/N2) residual (per meg)
30
20
10
0
−10
−20
−30
−20
−15
−10
−5
0
5
10
15
20
4:1 slope
δ(Ar/N2) residual (per meg)
δ(O2/N2) residual (per meg)

Figure 10.

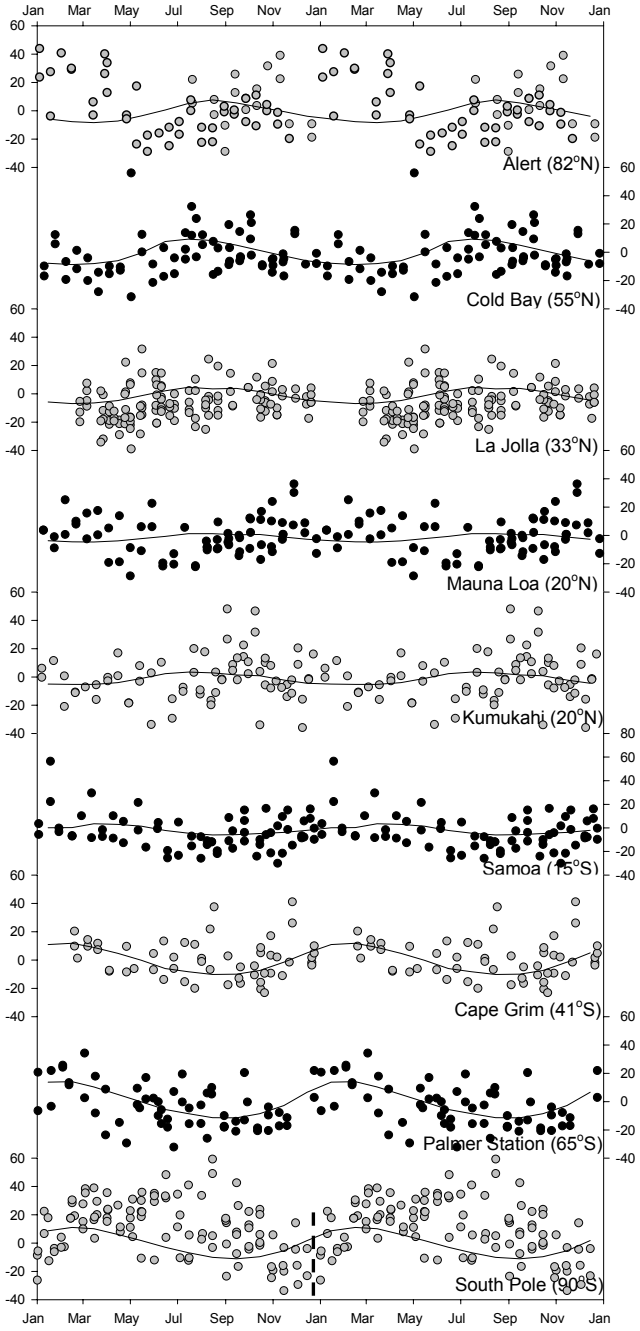
Jan Mar May Jul Sep Nov Jan Mar May Jul Sep Nov Jan
Alert (82°N)
Cold Bay (55°N)
La Jolla (33°N)
Mauna Loa (20°N)
Kumukahi (20°N)
Samoa (15°S)
Cape Grim (41°S)
Palmer Station (65°S)
South Pole (90°S)

Figure 11.